Nuclear Engineering and Technology 51 (2019) 894–903

Contents lists available at ScienceDirect

Nuclear Engineering and Technology

journal homepage: www.elsevier.com/locate/net

Original Article

Fragility assessment for electric cabinet in nuclear power plant using response surface methodology

Thanh-Tuan Tran [a, b], Anh-Tuan Cao [a], Thi-Hong-Xuyen Nguyen [a], Dookie Kim [a, *]

[a] Civil and Environmental Engineering, Kunsan National University, Daehak-ro, Gunsan-si, Jeollabuk-do, 558, Republic of Korea
[b] Faculty of Technology and Technique, Quy Nhon University, Viet Nam

ARTICLE INFO

Article history:
Received 14 September 2018
Received in revised form
27 November 2018
Accepted 29 December 2018
Available online 29 December 2018

Keywords:
Fragility curve
Seismic intensity measure
System identification
Lognormal assumption
Average spectral acceleration
Linear regression

ABSTRACT

An approach for collapse risk assessment is proposed to evaluate the vulnerability of electric cabinet in nuclear power plants. The lognormal approaches, namely maximum likelihood estimation and linear regression, are introduced to establish the fragility curves. These two fragility analyses are applied for the numerical models of cabinets considering various boundary conditions, which are expressed by representing restrained and anchored models at the base. The models have been built and verified using the system identification (SI) technique. The fundamental frequency of the electric cabinet is sensitive because of many attached devices. To bypass this complex problem, the average spectral acceleration ($S_{\overline{a}}$) in the range of period that cover the first mode period is chosen as an intensity measure on the fragility function. The nonlinear time history analyses for cabinet are conducted using a suite of 40 ground motions. The obtained curves with different approaches are compared, and the variability of risk assessment is evaluated for restrained and anchored models. The fragility curves obtained for anchored model are found to be closer each other, compared to the fragility curves for restrained model. It is also found that the support boundary conditions played a significant role in acceleration response of cabinet.

1. Introduction

Electric cabinet is one of the most popular components in the nuclear industry, which contains many power distribution systems such as electric switchboard, control transformer, or control circuit fuse, etc. Thus, the evaluation of seismic vulnerability for either this equipment [1] or nuclear power plants (NPPs) [2] should be considered carefully. In order to assess the seismic damage of electric cabinet with its devices, fragility analysis is a useful method [3,4]. Fragility curve estimates the probability of structural damage due to earthquakes as a function of an intensive measure of the ground motion.

Over the past decades, many significant researches for fragility analysis have been carried out, which are used for different aims such as collapse risk assessment [5,6], design checking [7] or assessing potential effects and risks, including functional and loss in economic and lives [8,9], etc. The fragility curves can be generated based on the following methods: (i) expert-based or judgmental, (ii) empirical, (iii) analytical, and (iv) hybrid methods. Each method has the pros and cons which was presented in the work of Billah and Alam [10]. In the present study, the lognormal cumulative distribution function is used as a typical approach for conducting fragility analysis [3,11]. The parameters of median and the standard deviation (denoted as θ and β, respectively) are determined either by maximum likelihood estimation [12,13] or by fitting a linear regression-based probabilistic model [14,15].

One of the challenges for the seismic fragility analysis is the selection of a ground motion intensity measure (IM). Commonly, in PBEE, the peak ground motion (PGA) [9] and the spectral acceleration at the first period ($S_a(T_1)$) [16], or the spectral displacement (S_d) are selected as IMs. Other IMs such as peak ground displacement (PGD) and peak ground velocity (PGV) can be chosen also. However, one of the requirements for selecting IM is to avoid the large dispersion in the response. Because many devices are installed inside the cabinet, the fundamental frequency of components are sensitive to their response. For example, the sensitivity of acceleration response depends on the locations of circuit breakers or fusible switches, while the displacement at the top of the equipment is controlled by conduits connection. To solve this

* Corresponding author.
E-mail addresses: tranthanhtuan@hotmail.com.vn (T.-T. Tran), anhtuan.hcmut@gmail.com (A.-T. Cao), xuyennguyen1092@gmail.com (T.-H.-X. Nguyen), kim2kie@kunsan.ac.kr (D. Kim).

https://doi.org/10.1016/j.net.2018.12.025

complex problem, many researchers have been suggested using the average spectral acceleration ($S_{\overline{a}}$) in the range of period [17,18]. Eads et al. [19] used $S_{\overline{a}}$ as an IM for collapse risk assessment of 700 moment-resting frame and shear wall structures of various height level to compare the efficiency and sufficiency of IMs.

To construct the fragility curves, finite element models (FEMs) of cabinet were built in SAP2000. These models considering the effects of various boundary conditions, namely restrained and anchored model, which were applied to perform the nonlinear behaviors of the structure [20–22]. The models have been verified using the system identification (SI) technique. This is a process for developing and updating model of structure rely on the input and output experimental data [23,24]. It can also be used to "realize" the mathematical dynamic model that can predict the measured output data from the measured input excitation. In addition, SI refers to process for estimating the dynamic properties of a structural system from its measured data and in this case is the cabinet of nuclear power plant. In this study, the response surface methodology (RSM) [25], which is used popular as a tool in order to optimize the FE model has been applied [26]. The central composite design (CCD) based on RSM has been used to design the sample of the experiment considering input parameters. CDD contains an embedded factorial or fractional factorial design with center points augmented with a group of 'star points' that allow estimation of curvature. The design sample is employed to compare the output natural frequency and three-dimensional (3D) FEM mode shape of cabinet with measured results. Result in, the model is optimized by CCD provides adequate accuracy and computational efficiency for identifying the physical condition of the structure.

In this paper, fragility curves based on the lognormal shape are introduced for cabinet and the $S_{\overline{a}}$ is proposed as a practical and efficient IM for estimating the collapse of cabinet. The effects of various support boundary conditions including restrained and nonlinear anchored are also investigated. A process of risk assessment, shown in Fig. 1, was established to evaluate the vulnerability of electric cabinet in nuclear power plants. Results in, collapse risk assessment show better agreement in anchored model than restrained model.

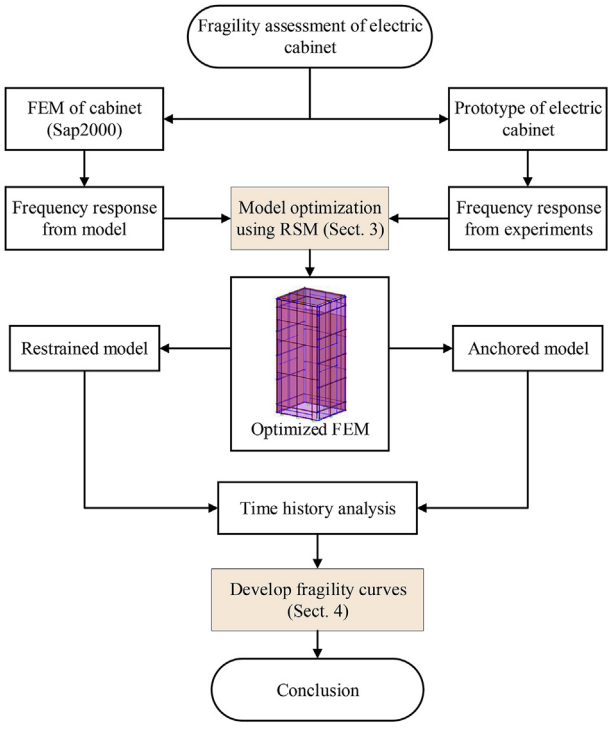

Fig. 1. Procedure of risk assessment in this study.

2. Numerical model of cabinet

2.1. Specification of electric cabinet

This research uses a prototype of electric cabinet (Fig. 2(a)) that its parameters are provided INNOSE Tech Company in Korea. The dimensions of cabinet are 800 × 800 × 2100 (mm × mm × mm) and its weight is 287 kg, while the door's weight is 43.6 kg for each one. The main sections of frames are rectangular and C-shape that are used for the main-frame and sub-frame of structure. The shape of frame sections and their parameters are displayed in Fig. 2(c). The thickness of steel panels is 2.3 mm. All frame and plate members are assigned the SS400 steel with 200 GPa of modulus of elastic, the density (ρ) and Poisson's ratio (ν) are 7850 kg/m^3 and 0.3, respectively. Welding is used to connect the frame with the plates in the prototype of electric cabinet. To investigate the dynamic characteristic of the cabinet, the experiment vibration test is conducted for the cabinet, which is mounted on a shaking. The modal parameters are derived from the shaking table test using the frequency domain decomposition (FDD) [27] method as given in Table 1.

The FEM of cabinet are generated using SAP2000, as shown in Fig. 2(b). The models are built using the frame and shell elements. In order to get accurately model, the model should be composed closely with the real behavior of cabinet. Therefore, the connections between the plates and frame are simulated as rigid link element. The hinge between door and frame are also considered to be fixed at five degrees of freedom, only the rotation around the hinge axis is released. For the support boundary condition, the fully fixed connection is assigned at the base of cabinet. Through the modal analyses, the natural frequencies from the FEM are evaluated and compared with the experiment results, as shown in Table 1. Based on the results, the frequencies might have been reasonable because they have a good agreement each other. This model will be optimized using the SI technique that is explained in Section 3.

2.2. Numerical models for nonlinear support boundary condition

The support boundary conditions for switchboard cabinets examined by previous section are assumed fully fixed at the base. However, the bolt connection presents the most common boundary condition in the practice, leading to rocking behavior during excitations. Therefore, to get enhanced understanding the dynamic characteristics of the cabinet with various boundary conditions, the anchored model considering the stiffness of connection is proposed. A total of eight links represented for eight bolts (two points at the left and right sides, and six points at front and back sides) is installed at the base of cabinet. The bolt connections are considered as a link at the base of the structure. When the base of the cabinet is anchored to the floor, the nonlinear behaviors the between cabinet and the support boundary may occur during the earthquake excitation.

Linear force-deformation relationship of connections is implemented for the FEM model. The characteristic of these connections depend on the various parameters such as the size of bolt and washer, the size and thickness of member. Therefore, the nonlinear properties of this connection can be calculated. The stiffness of anchor bolt is calculated based on a simplified pressure-cone method as presented by Shigley [28]. The initial stiffness of the bolt 495.1 × 10^3 kN/m is applied for link elements.

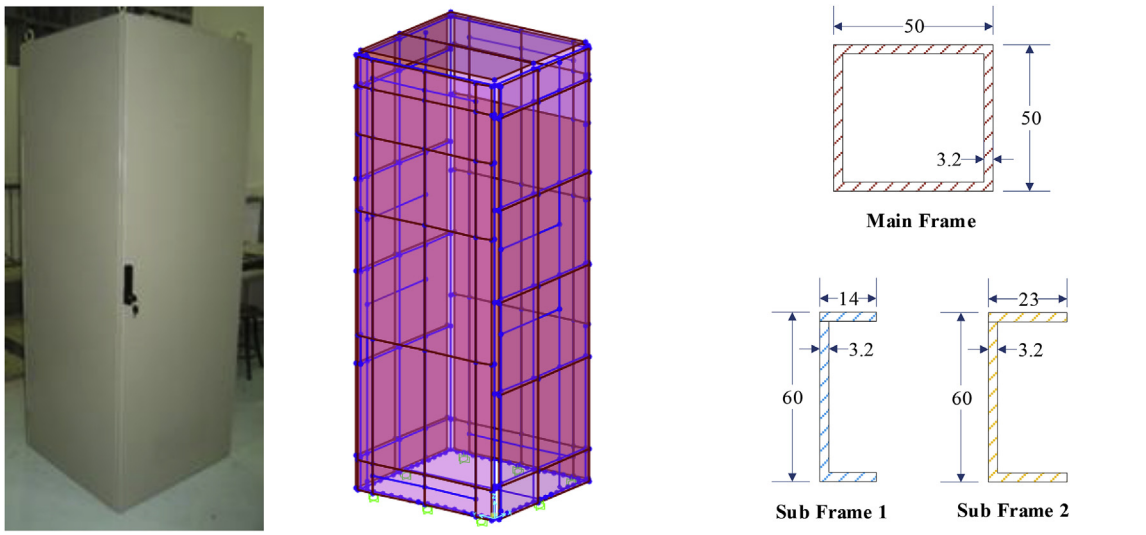

(a) Appearance model (b) Finite element model (c) Sections of frame elements (unit: mm)

Fig. 2. Model of electric cabinet.

Table 1
The natural frequencies of cabinet (Hz).

Mode Shape	Mode	Test	FEM
Front-Back	1	14.75	14.36
	2	25.87	23.58
Side-Side	1	16.63	14.64
	2	44.75	43.77

3. System identification of cabinet

3.1. Methodology for system identification

The response surface methodology (RSM) is a collection of statistical and mathematical models which are convenient for modelling, analyzing, optimization and building empirical model [29]. Summary of stages for optimization by RSM approach in this work are displayed in Fig. 3. The process is divided into five stages: (1) selection of output response and input factors, (2) chosen the design strategy, (3) execution the obtained results, (4) fitting the model and (5) verification of the model based on the optimal conditions.

Rely on a series of tests, called runs, RSM investigates the relationship between the several explanatory variables (x) and one or more response variables (b) of structure.

$$b = f(a_1, a_2, \ldots a_n) + u \tag{1}$$

where u describe the noise and error observed (offset term) in the response b and $f(a_1, a_2, \ldots a_n)$ represents the response of structure due to the sets of input variables. By using design of experiments, the optimization of response (output variables) will be obtained from several independent variables (input variables). There are two equations commonly used to describe the magnitude of the coefficients including linear and polynomial equation which are as follows:

First order liner equation:

$$b = \beta_0 + \sum_{i=1}^{n} \beta_i a_i + \sum_{i,j=1}^{n} \beta_{ij} a_i a_j + u \tag{2}$$

Second order polynomial equation:

$$b = \beta_0 + \sum_{i=1}^{n} \beta_i a_i + \sum_{i=1}^{n} \beta_i a_i^2 + \sum_{i,j=1}^{n} \beta_{ij} a_i a_j + u \tag{3}$$

where b is the predicted response; β_0, β_i and β_{ij} are the estimated partial regression coefficient of noise, a_i is the coded factor

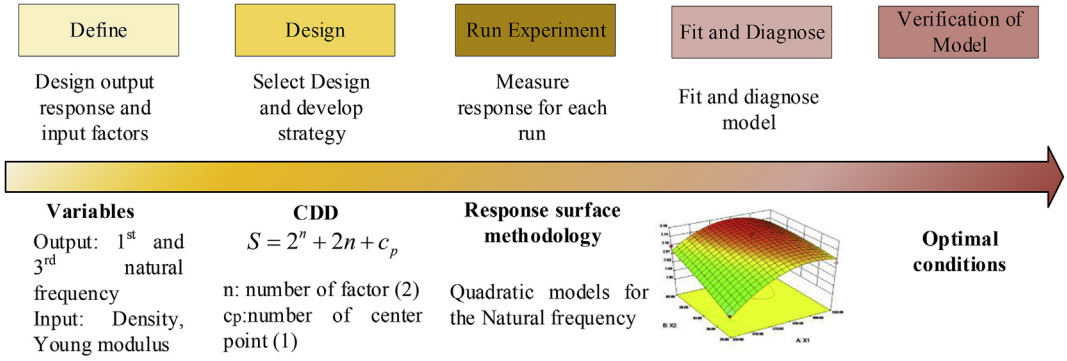

Fig. 3. Flowchart of optimization in RSM.

$(i, j = 1, 2, 3 \ldots, n)$ and u is the offset term. The polynomial equation can be extended to higher order, but in general for solving engineering problem second order is adequate. In this paper, CCD is used for identifying the structural parameters.

The central composite design (CCD) is a tool of design experiment for optimization of response (output variables) [30]. The CCD can be effective to predict the output by using the first order and second order polynomial equation relying on central and axial points with factorial design. The total number of experiments are created by using CCD computed by the following equation:

$$S = 2^n + 2n + c_p \tag{4}$$

where n is the number of factor and c_p is the number of center-point, in this case: The number of experiments is $S = 2^2 + 2 \times 2 + 1 = 9$.

3.2. RSM based identification results

It is apparently undeniable that first three vibration modes typically constitute the major contribution of the dynamic responses of the structure. Around 80% structural mass of the entire cabinet supported structure is governed by the first three modes. Considering the natural frequency of cabinet following x and y direction, therefore, the first and third mode have been considered to control under random vibration. Moreover, to enhance the exact behaviors of cabinet, the optimization based on response surface methodology (RSM) has been applied.

For this purpose, an experiment has been proceed based on RSM coupled with CCD to investigate the factors affecting responses of cabinet. Natural frequency amplitude of 1st front-back $(NF_{1,FB})$ and 1st side-side $(NF_{1,SS})$ mode has been counted as a structural response. This structural response has been considered as an objective function, where Young's modulus and the density have been taken as an independent variable for the cabinet. The objective function illustrates in Eq. (5).

$$F_k = (NF_k) \tag{5}$$

Where NF_k, $k = 1, 3$ is the natural frequency of cabinet at mode k. For optimizing the natural frequency from the analysis of design experiment value, Young's modulus and density have been used as design variables of cabinet and structural analysis has been executed to get the structural response.

The sets of experiments have 9 experimental points composed of 4 factorial points, 4 axial points and 1 center point which have been created randomly with given interest region of Young's modulus and the density [31]. The interest region of variables is shown in Table 2.

Table 3 describes either the analysis point and structural responses corresponding to these parameters or the sets of input parameters and output responses used for obtaining the response surface model. The Young's modulus (E) and density (ρ) indicate that the analysis point and natural frequency of the $NF_{1,FB}$ and $NF_{1,SS}$ are the corresponding structural responses.

In order to estimate the structure response, model equations are developed by design matrix including the quadratic term. Rely on the multiple linear regression, the variable coefficients have been obtained $b = P \times c$, where b is the predicted response, P is the product of the design matrix, and c is the corresponding coefficient. Through the coefficients, it is possible to know the characteristic of various factors influencing the response of various models. In addition, the second order polynomial equation including different combination factors help to visualize the output response which is illustrated in Table 4.

For easily understanding, a surface plot function has been applied to show 3D view of response due to changing combination of factors. Fig. 4 portrays the structural response plotted along with the two factors of steel material. Response optimizer function based on RSM has been used to optimize structural performances. For optimization cases of cabinet parameters, the natural frequency values have been targeted to minimize. The optimization mainly based on the target value set up to find out the enrich results. The final optimal Young's modulus and density ρ for material are 224.391 GPa and 7857.5 kg/m^3, and the value of natural frequency after using optimal parameters are listed in Table 5.

Table 2
Experiment regions.

Factor	Interest region		
	Low	Center	High
Young's modulus (MPa)	200000	222500	245000
Density (kg/m^3)	7850	7855	7860

Table 3
The analysis points and corresponding structural responses.

Run order	Pt Type	Analysis point		Structural responses	
		E	ρ	$NF_{1,FB}$	$NF_{1,SS}$
1	1	200000	7850	13.94	14.62
2	1	245000	7860	15.42	16.18
3	1	245000	7850	15.43	16.19
4	0	222500	7855	14.69	15.42
5	−1	222500	7847.93	14.70	15.43
6	−1	222500	7862.073	14.69	15.41
7	−1	190680.19	7855	13.60	14.28
8	−1	254319.81	7855	15.71	16.49
9	1	200000	7860	13.93	14.62

4. Risk assessment using the average spectral acceleration

The flowchart in Fig. 5 shows the analysis strategy of risk assessment procedure in this work. More details of the key components are given in the following processes. Initially, the suite of ground motion was chosen and applied in the nonlinear time history analysis for optimized models. Details of selected earthquake records are provided in Table 6 and the optimized models have been conducted in the previous chapter. The simulations were carried out on the cabinets in the two orthogonal horizontal directions. The next stage explains the choice of parameters for developing the fragility curves including the ground motion measures (as explained in Section 4.1) corresponding to the structural demand (as explained in Section 4.2). Then, the collapse risk assessment is performed based on the lognormal approaches including maximum likelihood estimation and linear regression (see in Section 4.3) to determine the median and the standard deviation. Finally, these outputs are obtained and used for developing the collapse fragility curves.

4.1. Intensity measure (IM) selection

As described above, the PGA, PGV, PGD or S_a are usually chosen

Table 4
Quadratic models for the natural frequencies.

Mode	Modal equation
$NF_{1,FB}$	$57 + 0.66 \times 10^{-4} E - 0.013\rho + 0.01 \times 10^{-4}\rho^2$
$NF_{1,SS}$	$60 + 0.69 \times 10^{-4} E - 0.013\rho + 0.01 \times 10^{-4}\rho^2$

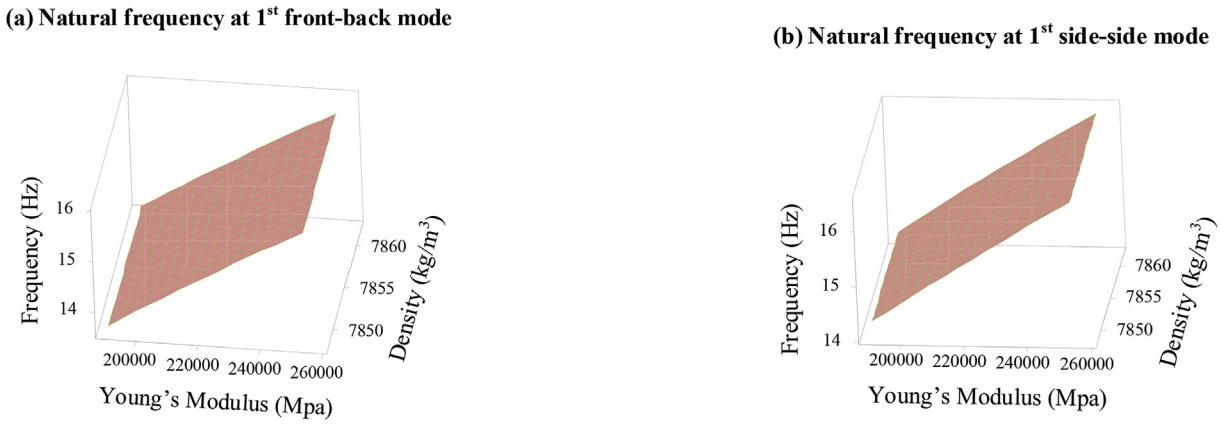

Fig. 4. Response surface plot.

Table 5
The errors of natural frequencies.

	Structural responses (Hz)		Error (%)	
	$NF_{1,FB}$	$NF_{1,SS}$	$NF_{1,FB}$	$NF_{1,SS}$
Before Optimizing	14.36	14.64	0.03	0.12
After Optimizing	14.75	15.5	0.00	0.07

as an intensity measures in seismic fragility analysis in engineering applications. These IMs have the pros and cons when being applied to components in nuclear power industry. As mentioned in the NUREG [32], the response of frequency-sensitive component in the electric cabinet is an important factor, which should be considered carefully for evaluating the dynamic characteristics. The PGA is a good index of peak acceleration in the time history, but it is not clear how to take the correlation between the input data with the fragility function for a frequency-sensitive component. S_a would also be a good index at a period for frequency-sensitive component, but it may not be practical to estimate the fragility of complex cabinets. Therefore, the $S_{\bar{a}}$ becomes the proposed IM to overcome the drawbacks. The $S_{\bar{a}}$ was first introduced by Cordova et al. [33] which is defined as geometric mean of two S_a components at range of the interesting period:

$$S_{\bar{a}}(T_i) = \left[\prod_{i=1}^{n} Sa(\mathrm{T_i})\right]^{1/n} \tag{6}$$

Where, n is number of periods of interest used for determining the $S_{\bar{a}}$ that frequency range of interest for electric cabinet ranges from 4 to 16 Hz [32].

The recorded dataset for the collapse risk assessment were selected from the PEER NGA database [34], including 40 ground motions with two components in each records, which are listed in Table 6. These earthquakes were recorded on the soil sites with the shear wave velocity ($V_{s,30}$) ranging from 360 m/s to 760 m/s with no consistent about faulting. These records cover the range of

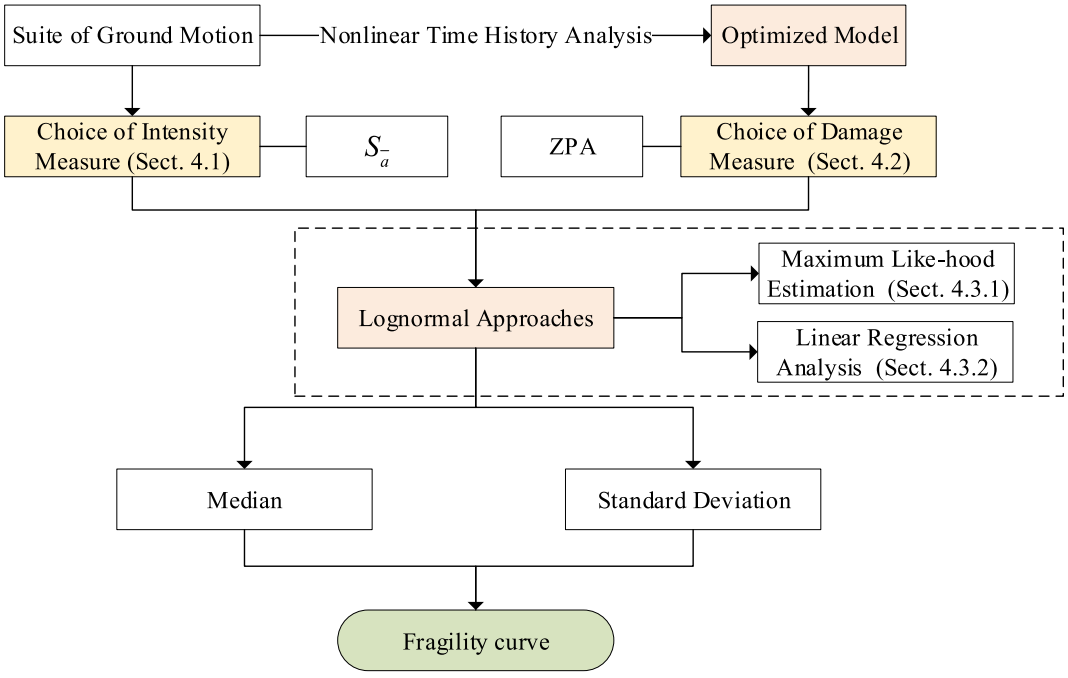

Fig. 5. Framework for collapse risk assessment of cabinet using average spectral acceleration.

Table 6
Details of ground motion selection.

No	Earthquake Name	Year	Magnitude	R_{RUP}(km)	$V_{s,30}$ (m/sec)
1	Helena_ Montana-01	1935	6	2.86	593.35
2	Kern County	1952	7.36	125.59	415.13
3	Southern Calif	1952	6	73.41	493.5
4	Parkfield	1966	6.19	17.64	408.93
5	Borrego Mtn	1968	6.63	207.14	415.13
6	San Fernando	1971	6.61	173.16	360.45
7	Friuli_ Italy-01	1976	6.5	49.38	496.46
8	Tabas_ Iran	1978	7.35	120.81	377.56
9	Imperial Valley-06	1979	6.53	15.19	471.53
10	Mammoth Lakes-01	1980	6.06	6.63	382.12
11	Victoria_ Mexico	1980	6.33	14.37	471.53
12	Irpinia_ Italy-01	1980	6.9	52.94	612.78
13	Irpinia_ Italy-02	1980	6.2	29.86	476.62
14	Corinth_ Greece	1981	6.6	10.27	361.4
15	Coalinga-01	1983	6.36	42.92	522.74
16	Ierissos_ Greece	1983	6.7	65.67	463.92
17	Taiwan SMART1 (25)	1983	6.5	92.04	671.52
18	Borah Peak_ ID-01	1983	6.88	100.22	445.66
19	Morgan Hill	1984	6.19	3.26	488.77
20	Nahanni_ Canada	1985	6.76	9.6	605.04
21	San Fernando	1971	6.61	109.73	443.85
22	Imperial Valley-06	1979	6.53	24.61	362.38
23	New Zealand-02	1987	6.6	16.09	551.3
24	Superstition Hills-02	1987	6.54	5.61	362.38
25	Loma Prieta	1989	6.93	41.88	391.91
26	Loma Prieta	1989	6.93	52.53	517.06
27	Cape Mendocino	1992	7.01	6.96	567.78
28	Landers	1992	7.28	69.21	382.93
29	Northridge-01	1994	6.69	36.77	549.75
30	Northridge-01	1994	6.69	68.93	501.75
31	Northridge-01	1994	6.69	47.98	544.68
32	Duzce_ Turkey	1999	7.14	168.26	399.61
33	Caldiran_ Turkey	1976	7.21	50.82	432.58
34	Hector Mine	1999	7.13	166.11	375.16
35	Hector Mine	1999	7.13	43.05	382.93
36	Hector Mine	1999	7.13	74.92	436.14
37	Montenegro_ Yugoslavia	1979	7.1	66.67	585.04
38	El Mayor-Cucapah_ Mexico	2010	7.2	45.47	523.99
39	Darfield_ New Zealand"	2010	7	124.96	586.28
40	Darfield_ New Zealand	2010	7	102.33	586.28

magnitude from 6.0 to 7.5 and the closet ruptured distance (R_{RUP}) ranges from 2.86 to 207.14 km, as illustrated by scatter diagram in Fig. 6(a). The associated spectral accelerations of record suite are displayed in Fig. 6(b). In this article, only horizontal excitations are considered at the base of the cabinet.

4.2. Damage measure (DM) selection

Generally, response of structure can be evaluated by engineering demand parameters (EDPs), which are useful to predict the damage to structural and non-structural components [23]. Although previous researches have defined various damage levels (DS) and corresponding quantities to specify them. The damage limit states in seismic fragility analysis can be employed as maximum displacement at the peak of the structure (θ_{max}) [35], the inter-story drift ratio (θ) [36], stress for evaluating the EDPs. Determining these limit values considering damage measures vary on different structures, example bridges, wind turbine or nuclear power plant components.

The U.S. Nuclear Regulatory Commission document entitled

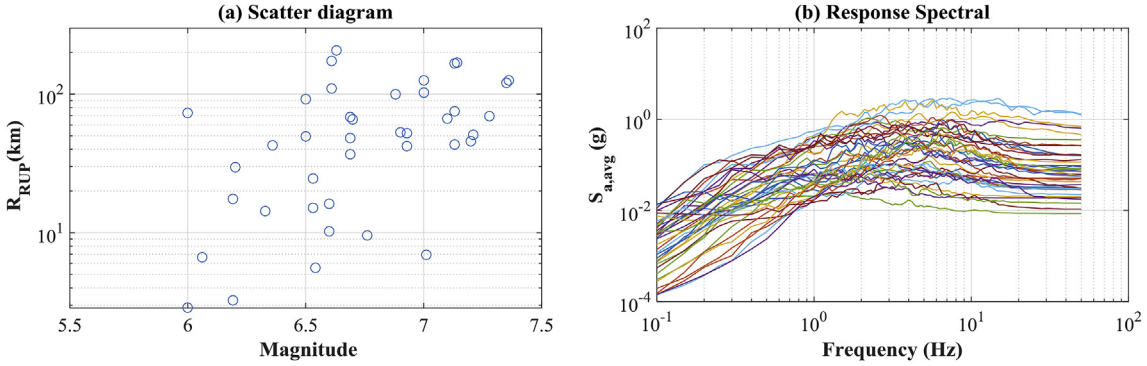

Fig. 6. Characteristics of selected ground motions.

Seismic Fragility Nuclear Power Plant Components (Phase II) [32] provides probabilistic fragility levels with electrical equipment of nonstructural components in NPPs by using shaking table tests. This report has collected existing test data and is applying the methodology to determine the fragility levels of equipment in NPPs. The data has been evaluated for four equipment classes, namely motor control center, switchboard, panel-board and power supply. Fragility levels have been determined for several failure modes of electric equipment, and suggested effective engineering demands (response demands) for the fragility functions such as acceleration response for cabinet. Based on this guideline, the acceleration response is chosen to be a critical engineering demand parameter to apply the fragility analysis since it can be determined analytically with reasonable accuracy. The DS related to the zero period acceleration at 2% damping and this value is defined when the zero period acceleration (ZPA) comes to 1.8 g. ZPA is the response acceleration value when time period of cabinet is zero.

4.3. Seismic fragility analysis

Seismic fragility analysis has been widely used to evaluate seismic capacities of components in nuclear power plants. Fragility curves is a statistical tool representing the probability of exceeding a given DS as a function of an engineering demand parameter that represents different intensity level [37]. In this study, the lognormal approach is used as classical approach for developing the fragility curves and it is expressed in following equation:

$$Fragility = P[LS < D|IM] \tag{7}$$

Where, where LS is the limit state or damage level of the electrical equipment; IM is the earthquake intensity measure.

4.3.1. Maximum likelihood estimation (MLE)

The cumulative distribution of a lognormal function is used to define a fragility curves. In the present study, the fragility curves are conducted by a particular DS given the average spectral acceleration, $S_{\bar{a}}$. Thus, the fragility function can be written as follows:

$$P(DS|S_{\bar{a}}) = \Phi\left[\frac{1}{\beta}\ln\left(\frac{S_{\bar{a}}}{\theta}\right)\right] \tag{8}$$

In which P is the probability that a GM with $S_{\bar{a}} = x$ will cause the structure to collapse, $\boldsymbol{\theta}$ and $\boldsymbol{\beta}$ are the median and the standard deviation of the intensity measures, respectively; $\Phi[.]$ is the standard normal cumulative distribution function (CDF). The maximum likelihood estimation is proposed in the work by Shinozuka et al. [3]. Assumption that the $Sa_{avg} = x_j$ for each ground motion is independent, the likelihood function of the entire data set is taken from the Bernoulli distribution as follows:

$$Likelihood = \prod_{i=1}^{m}\left[P\left(DS\middle|S_{\bar{a},i}\right)\right]^{p_i}\left[1 - P\left(DS\middle|S_{\bar{a},i}\right)\right]^{1-p_i} \tag{9}$$

where m is the number of $S_{\bar{a}}$ levels and Π denotes the product over all levels; p depending on the thing that the limit state is exceed or not, and takes the value 1 or 0, respectively. The fragility function parameters, θ and β, are obtained by maximum the likelihood function [38].

$$\left\{\hat{\theta},\ \hat{\beta}\right\} = \arg\max_{\theta,\beta}(\ln(Likelihood)) \tag{10}$$

4.3.2. Linear regression (LR)

The probabilistic seismic demand model relates to the structure response quantity of interest (herein acceleration response) to an intensity measure of the earthquake motion. Cornell et al. [39] suggested a seismic demand model using a power function as described in Eq. (11):

$$D(S_{\bar{a}}) = a \bullet (S_{\bar{a}})^b \bullet \varepsilon \tag{11}$$

In which, ε is a lognormal random variable with a median of 1 and a logarithmic standard deviation $\beta_{D|S_{\bar{a}}}$; a and b are model parameters estimated using a liner regression analysis for the seismic demand model in the transformed logarithmic space in the following form:

$$\ln(D(S_{\bar{a}})) = \ln(a) + b\ln(S_{\bar{a}}) + \varepsilon \tag{12}$$

where $\ln(D(S_{\bar{a}}))$ is the expected value for the natural logarithm of DS given $S_{\bar{a}}$. The demand model is described as a straight line from a log-log plot of IM-DM relationship with dispersion of $\beta_{D|S_{\bar{a}}}$ describing the uncertainty in their relationship. Parameter $\beta_{D|S_{\bar{a}}}$ is obtained as logarithmic standard deviation of errors, which expressed in Eq. (13)

$$\beta_{D|S_{\bar{a}}} = \sqrt{\sum_{i=1}^{N}(e_i)^2 \Big/ (N-2)} \tag{13}$$

where e_i is the residual between the actual value $\ln(D_i)$ and the value predicted by the linear model. Result in, the fragility function from Eq. (7) with the median $\theta_m = \exp[(\ln(DS) - \ln(a))/b]$ is rewritten as follows:

$$P(DS|S_{\bar{a}}) = \Phi\left[\frac{\ln\left(\frac{S_{\bar{a}}}{\theta_m}\right)}{\frac{\beta_{D|S_{\bar{a}}}}{b}}\right] \tag{14}$$

5. Analysis results and discussions

Results of the fragility curves for two models of cabinet are presented and discussed in this section. The procedure is conducted for two FEM models with different boundary conditions including (1) the restrained model with fully fixed condition at the base and (2) the anchored model with the force-deformation relationships to the floor. The structural model is initially subjected to gravity load in all cases. Then, nonlinear time history analyses for 40 ground motions were performed on the cabinets in the two orthogonal horizontal directions. The acceleration response (Δ) at the top of cabinet is measured as a damage measure for assessment of collapse risk.

5.1. Effects of boundary condition on the behavior of cabinet

Fig. 7 displayed the paired data $(\ln S_{\bar{a}}, \ln\Delta)$ and the linear regression curve for two cabinet models and for the suite of records in Table 6. The data were partitioned into two parts: (1) blue-point data represent the structure without collapse and (2) red-point data describe the collapse of structure. It is obvious to note that the cloud data (blue-points) are not only covering a range of $S_{\bar{a}}$ value but also providing the total of collapse points in the range of $DS > 1.8g$. Additionally, the characteristics of the curves in term of coefficient $\ln(a)$, logarithmic slope b and associated dispersion $\beta_{D|S_{\bar{a}}}$ of the regression line from Eq. (12) for structural response are presented in the figure as well. It is also observed that the b -value

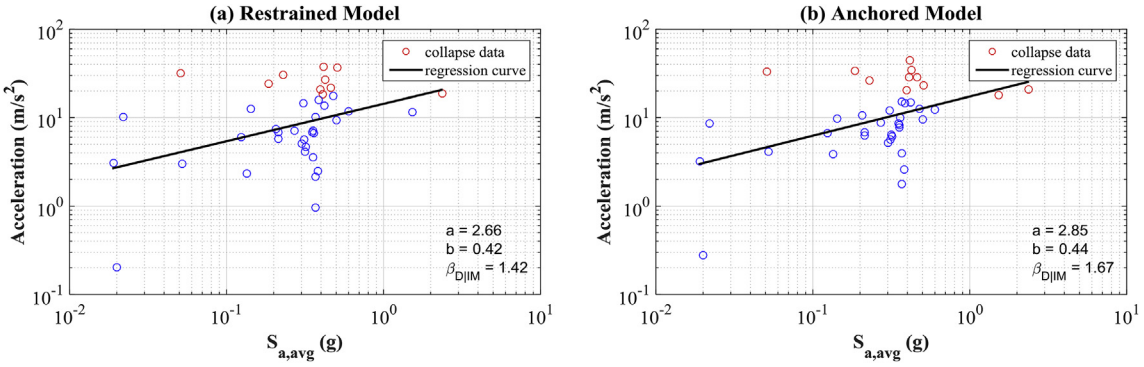

Fig. 7. Scatter plots and regression curves in log-scale.

of two boundary conditions is similar together (~0.4); whereas, the b -value for the restrained model (0.42) is smaller than those of the anchored model. The obtained results indicate that the sensitivity of boundary condition in the dynamic response of cabinet strucutre.

Based on the obtained results in Fig. 7, the correlation coefficient R^2 of the fitted linear model is used as a statistical measure for calculating the strength of the relationship between the relative movements of the two parameters ($\ln S_{\overline{a}}$, $\ln\Delta$). These values are 0.180 and 0.217 for restrained and anchored model, respectively. It shows that there is a stronger relationship in the anchored model than those of the restrained model. Furthermore, the acceleration responses of the anchored model are higher than the respective responses in restrained model since IM increases; this increase is accompanied by high values of dispersion, as expected. This is attributed to rocking behavior observed in the anchored model. Therefore, it is significant to note that consideration the boundary condition in cabinet structure is necessary to capture the vulnerable trend in the performance the electrical equipment.

The residuals that estimates of experimental error obtained by subtracting the observed responses from the predicted responses are displayed in order to evaluate the obtained cloud data (Fig. 7). The histogram and fitted normal distribution of residuals are showed in Fig. 8, while Fig. 9 illustrates the normal probability graph created from the same group of residuals used for Fig. 8. Small departures from the straight line in the normal probability plot for two models are common. However, the breaks near the middle of restrained model are also indications of abnormalities in the residual distribution which is shown clearly in Fig. 8. It is noted that in both figures, the anchored condition expresses a good linear fit of respective response with respect to IM in the lognormal scale.

5.2. Comparison of different fragility analysis methods

As described in Section 3, the fragility curves are calculated using the IDA results, which is mentioned in previous section and the results are obtained from the dynamic analysis. The acceleration response at the top of structural models are considered at multiple intensity level. The fragility curves of cabinet for two cases (restrained and anchored models) are considered and they are shown in Fig. 10. The corresponding median (θ) and dispersion (β) value of the fragility curve with the MLE and LR approach are summarized in Table 7. The median value expresses the position, where the fragility curve reaches the value of 0.5, whereas the dispersion is a measure of the steepness of the curve. It can be observed that the curves in the anchored model are close to each other than that exhibit in the restrained model. The difference between the median of the two approaches is more pronounced for both models. The median value in case of restrained model is greater than anchored model. For the former case, the value for LR-based fragility ($\theta = 1.541$) is smaller than that of the MLE-based fragility ($\theta = 1.861$). While for the latter case, the trend of median is reversed, which can see in Table 7 for this comparison.

One another observation between the obtained curves is the dispersion value that explain the uncertainty in the structural behavior. The β value for MLE-based curve in the restrained model is higher than the LR-based one; however, the trend is reversed for the anchored model (see in Table 7). The value in LR approach ($\beta = 0.665$) is found to be greater than MLE approach ($\beta = 0.546$) for the restrained model. On the other hand, β is found to be smaller at LR approach ($\beta = 0.582$) for anchored case.

Based on the obtained results, the curves are found depend on the method used to estimate the parameters of fragility function.

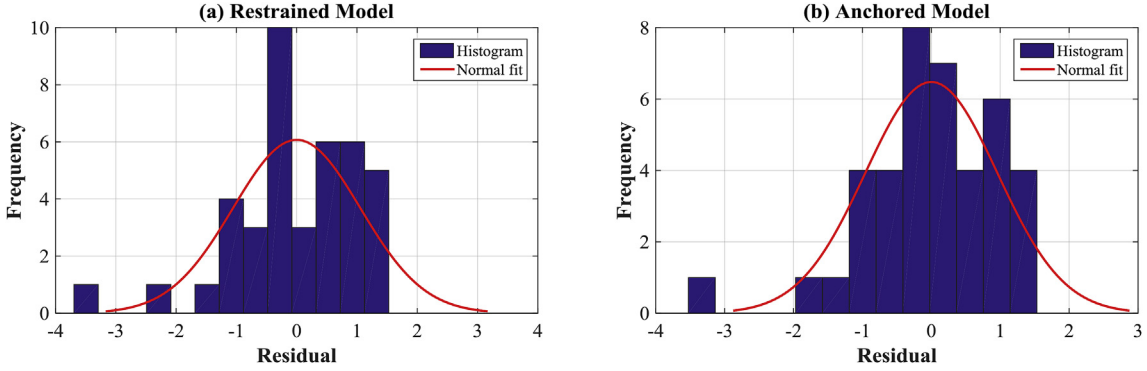

Fig. 8. Histogram and fitted normal distribution of residuals.

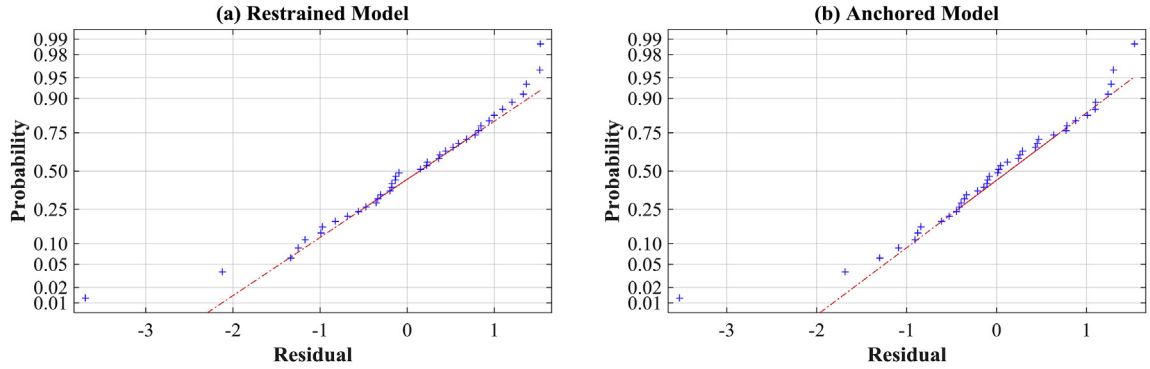

Fig. 9. Normal probability plot of residuals of two models.

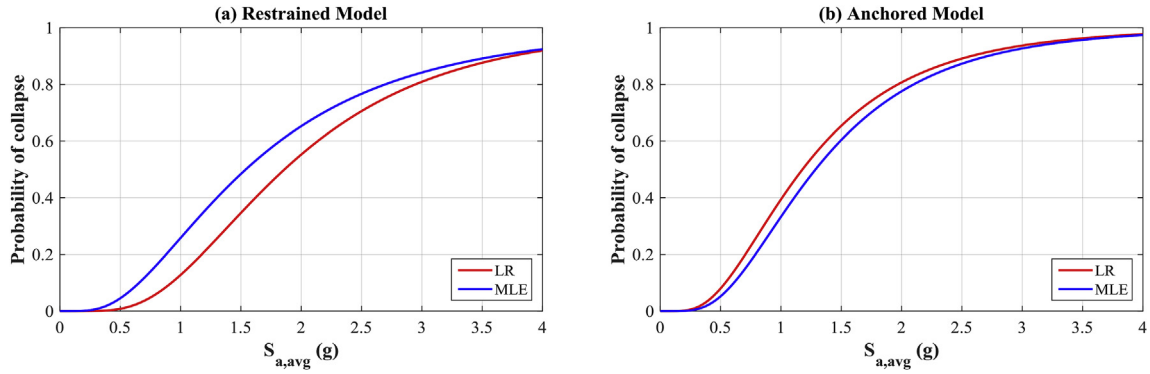

Fig. 10. Fragility curves.

Table 7
Median and dispersion value of fragility function.

Approach	Restrained model		Anchored model	
	θ	β	θ	β
MLE	1.861	0.546	1.179	0.610
LR	1.541	0.665	1.287	0.582

Note that in Section 4.3.2, the dispersion value for the fragility curve is assumed homoscedasticity property. In this study, homoscedasticity describes a situation that the error term (relationship between the independent variables, IM, and the dependent variable, DM) is the same across all values of the independent variables. Obviously, the assumption of normal distribution is not valid, this explains the different trend of fragility curves in LR approach of two restrained and anchored models. These findings are compatible with the fitted normal distribution in Fig. 8. The limitations of the LR approach have also been presented in the work by Jalayer et al. [40].

6. Conclusions

The fragility curves using the lognormal approach for electric cabinet in NPP has been investigated in this study. Two different fragility analysis methods, namely maximum likelihood estimation and linear regression, are applied for evaluating the seismic vulnerability of cabinet. The restrained and anchored models have been considered to assess the effects of boundary conditions to the structural response. Numerical models are optimized by using the system identification technique. These models are analyzed using nonlinear time history analysis with a set of 40 ground motions. The acceleration responses are considered as an engineering demand parameter for analyses. Based on the obtained results, the key conclusions can be drawn as follows:

- This study provides a framework for evaluating the seismic vulnerability for electric cabinet. This procedure starts from the generation and optimization of cabinet model. To carry out fragility analysis, the selection of ground motion dataset is important and it is relied on structural demands. The fragility analysis provides a feasible option to understand the dynamic behavior of cabinet in collapse risk assessment.
- The system identification technique based on the response surface methodology is applied to validate and calibrate the numerical model. The reliability of the results is mainly depended on the accuracy of model simulation. The Young's modulus and density are significant parameters, which are selected and used to optimize the model. The characteristic of the finite element model is also compared with the experimental data and this step is necessary to ensure that the model is reliable.
- The connection's stiffness at the base leads to the sensitivity of dynamic characteristics of the cabinet. This work also provides the expanded understanding about the effects of the support boundary conditions in structure, which is exhibited by the seismic response of facilities in nuclear power plant.
- For implementing the collapse risk assessment of the cabinet with a large number of time history ground motions, the $S_{\bar{a}}$ is evaluated as a suitable intensity measure for engineering demands in the electric equipment.
- The present study uses the lognormal cumulative distribution function to conduct a fragility analysis. However, the validity of this approach for the linear regression analysis case still remains

shortcomings. The fragility curves obtained from anchored model are found to be closer each other, compared to the fragility curves for restrained model.

Acknowledgments

The National Research Foundation of Korea Grant funded by the Korean Government (NRF-2018R1A2B2005519) supported this work.

Appendix A. Supplementary data

Supplementary data to this article can be found online at https://doi.org/10.1016/j.net.2018.12.025.

References

[1] J. Hur, E. Althoff, H. Sezen, R. Denning, T. Aldemir, Seismic assessment and performance of nonstructural components affected by structural modeling, Nucl. Eng. Technol. 49 (2) (2017) 387–394.
[2] T.T. Tran, T.H. Nguyen, D. Kim, Seismic incidence on base-isolated nuclear power plants considering uni-and bi-directional ground motions, J. Struct. Integr. Mainten. 3 (2) (2018) 86–94.
[3] M. Shinozuka, M.Q. Feng, H. Kim, T. Uzawa, T. Ueda, Statistical Analysis of Fragility Curves, 2003.
[4] A.S. Pisharady, P.C. Basu, Methods to derive seismic fragility of NPP components: a summary, Nucl. Eng. Des. 240 (11) (2010) 3878–3887.
[5] S. Kwag, D. Hahm, Development of an earthquake-induced landslide risk assessment approach for nuclear power plants, Nucl. Eng. Technol. 50 (8) (2018) 1372–1386.
[6] L. Eads, E. Miranda, H. Krawinkler, D.G. Lignos, An efficient method for estimating the collapse risk of structures in seismic regions, Earthq. Eng. Struct. Dyn. 42 (1) (2013) 25–41.
[7] A. Bakhshi, P. Asadi, Probabilistic evaluation of seismic design parameters of RC frames based on fragility curves, Sci. Iran. 20 (2) (2013) 231–241.
[8] M. Kohrangi, D. Vamvatsikos, P. Bazzurro, Site dependence and record selection schemes for building fragility and regional loss assessment, Earthq. Eng. Struct. Dyn. 46 (10) (2017) 1625–1643.
[9] N.N. Pujari, T.K. Mandal, S. Ghosh, S. Lala, Optimisation of IDA-based fragility curves, in: Safety, Reliab. Risk Life-cycle Perform. Struct. Infrastructures-proc. 11th Int. Conf. Struct. Saf. Reliab. ICOSSAR 2013, 2013, pp. 4435–4440.
[10] A.H.M. Muntasir Billah, M. Shahria Alam, Seismic fragility assessment of highway bridges: a state-of-the-art review, Struct. Infrastruct. Eng. 11 (6) (2015) 804–832.
[11] B.R. Ellingwood, Earthquake risk assessment of building structures, Reliab. Eng. Syst. Saf. 74 (3) (2001) 251–262.
[12] S. Günay, K.M. Mosalam, PEER performance-based earthquake engineering methodology, revisited, J. Earthq. Eng.. 17(6), 829-858.
[13] I. Zentner, Numerical computation of fragility curves for NPP equipment, Nucl. Eng. Des. 240 (6) (2010) 1614–1621.
[14] B.R. Ellingwood, K. Kinali, Quantifying and communicating uncertainty in seismic risk assessment, Struct. Saf. 31 (2) (2009) 179–187.
[15] S.H. Jeong, A.M. Mwafy, A.S. Elnashai, Probabilistic seismic performance assessment of code-compliant multi-story RC buildings, Eng. Struct. 34 (2012) 527–537.
[16] C.B. Haselton, J.W. Baker, A.B. Liel, G.G. Deierlein, Accounting for ground-motion spectral shape characteristics in structural collapse assessment through an adjustment for epsilon, J. Struct. Eng. 137 (3) (2009) 332–344.
[17] A.K. Kazantzi, D. Vamvatsikos, Intensity measure selection for vulnerability studies of building classes, Earthq. Eng. Struct. Dyn. 44 (15) (2015) 2677–2694.
[18] J.W. Baker, C. Allin Cornell, Spectral shape, epsilon and record selection, Earthq. Eng. Struct. Dyn. 35 (9) (2006) 1077–1095.
[19] L. Eads, E. Miranda, D.G. Lignos, Average spectral acceleration as an intensity measure for collapse risk assessment, Earthq. Eng. Struct. Dyn. 44 (12) (2015) 2057–2073.
[20] S.K. Kunnath, Modeling of reinforced concrete structures for nonlinear seismic simulation, J. Struct. Integr. Mainten. 3 (3) (2018) 137–149.
[21] P.C. Nguyen, S.E. Kim, Distributed plasticity approach for time-history analysis of steel frames including nonlinear connections, J. Constr. Steel Res. 100 (2014) 36–49.
[22] D.K. Kim, F. Wang, S. Chaudhary, Modal energy balance approach for seismic performance evaluation of building structures considering nonlinear behavior, J. Struct. Integr. Mainten. 1 (1) (2016) 10–17.
[23] M. Vejmelka, M. PALUŠ, K. ŠUŠMÁKOVÁ, Identification of nonlinear oscillatory activity embedded in broadband neural signals, Int. J. Neural Syst. 20 (02) (2010) 117–128.
[24] G. Puscasu, B. Codres, Nonlinear system identification and control based on modular neural networks, Int. J. Neural Syst. 21 (04) (2011) 319–334.
[25] F. Bayramov, C. Taşdemir, M.A. Taşdemir, Optimisation of steel fibre reinforced concretes by means of statistical response surface method, Cement Concr. Compos. 26 (6) (2004) 665–675.
[26] L.E. Chávez-Valencia, A. Manzano-Ramírez, E. Alonso-Guzmán, M.E. Contreras-García, Modelling of the performance of asphalt pavement using response surface methodology—the kinetics of the aging, Build. Environ. 42 (2) (2007) 933–939.
[27] R. Brincker, L. Zhang, P. Andersen, Modal identification of output-only systems using frequency domain decomposition, Smart Mater. Struct. 10 (3) (2001), 441.
[28] R.G. Budynas, J.K. Nisbett, Shigley's Mechanical Engineering Design, vol. 8, McGraw-Hill, New York, 2008.
[29] A.I. Khuri, S. Mukhopadhyay, Response surface methodology, Wiley Interdiscipl. Rev.: Comput. Stat. 2 (2) (2010) 128–149.
[30] B. Sadhukhan, N.K. Mondal, S. Chattoraj, Optimisation using central composite design (CCD) and the desirability function for sorption of methylene blue from aqueous solution onto Lemna major, Karbala Int. J. Modern Sci. 2 (3) (2016) 145–155.
[31] M. Hussan, M.S. Rahman, F. Sharmin, D. Kim, J. Do, Multiple tuned mass damper for multi-mode vibration reduction of offshore wind turbine under seismic excitation, Ocean Eng. 160 (2018) 449–460.
[32] NUREG, U.S. Nuclear Regulatory Commission, Seismic Fragility of Nuclear Power Plant Components [PHASE II], NUREG/CR-4659, BNL-NUREG-52007, vols. 2–4, Department of Nuclear Energy, Brookhaven National Laboratory, Long Island, NY, 1987.
[33] P.P. Cordova, G.G. Deierlein, S.S. Mehanny, C.A. Cornell, Development of a two-parameter seismic intensity measure and probabilistic assessment procedure, in: The Second US-Japan Workshop on Performance-based Earthquake Engineering Methodology for Reinforced Concrete Building Structures, 2000, pp. 187–206. September.
[34] PEER. PEER NGA, Database. Pacific Earthquake Engineering Research Center, University of California, Berkeley. California, 2006. http://peer.berkeley.edu/nga/.
[35] J. Alam, D. Kim, B. Choi, Uncertainty reduction of fragility curve of intake tower using bayesian inference and Markov chain Monte Carlo simulation, Struct. Eng. Mech. 63 (1) (2017) 47–53.
[36] M.S. Kirçil, Z. Polat, Fragility analysis of mid-rise R/C frame buildings, Eng. Struct. 28 (9) (2006) 1335–1345.
[37] R.P. Kennedy, M.K. Ravindra, Seismic fragilities for nuclear power plant risk studies, Nucl. Eng. Des. 79 (1) (1984) 47–68.
[38] J.W. Baker, Efficient analytical fragility function fitting using dynamic structural analysis, Earthq. Spectra 31 (1) (2015) 579–599.
[39] C.A. Cornell, F. Jalayer, R.O. Hamburger, D.A. Foutch, Probabilistic basis for 2000 SAC federal emergency management agency steel moment frame guidelines, J. Struct. Eng. 128 (4) (2002) 526–533.
[40] F. Jalayer, R. De Risi, G. Manfredi, Bayesian Cloud Analysis: efficient structural fragility assessment using linear regression, Bull. Earthq. Eng. 13 (4) (2015) 1183–1203.